Microchimica Acta (2021) 188:296
https://doi.org/10.1007/s00604-021-04959-y

ORIGINAL PAPER

Electrochemiluminescence paper-based screen-printed electrode for HbA1c detection using two-dimensional zirconium metal-organic framework/Fe_3O_4 nanosheet composites decorated with Au nanoclusters

Anita Ahmadi[1,2] · Seyyed Mehdi Khoshfetrat[3] · Shima Kabiri[1,2] · Parisa Seyed Dorraji[4] · Bagher Larijani[2] · Kobra Omidfar[1,2]

Received: 5 April 2021 / Accepted: 26 July 2021

Abstract

Glycated hemoglobin (HbA1c) is one of the most popular biomarkers which can be utilized for the diagnosis and control of diabetes in clinical practice. In this study, a sandwich paper-based electrochemiluminescence (ECL) biosensor has been developed using the zirconium metal-organic framework/Fe_3O_4(trimethyl chitosan)/gold nanocluster (Zr-MOF/Fe_3O_4(TMC)/AuNCs) nanocomposite as tracing tag to label anti-HbA1c monoclonal antibody and reduced graphene oxide (rGO) as immobilization platform of sensing element. The screen-printed electrodes (SPEs) were constructed and modified by sputtering a thick layer of gold on the paper substrate, followed by electrochemical reduction of aminophenylboronic acid (APBA)–functionalized GO to rGO/APBA, respectively. Different types of surface analysis methods were applied to characterize the Zr-MOF/Fe_3O_4(TMC)/AuNCs nanomaterials fabricated. Finally, antibody-labeled Zr-MOF/Fe_3O_4(TMC)/AuNCs nanocomposites were subjected to HbA1c in the sample and on the paper-based SPE. Quantitative measurement of HbA1c was performed using ECL and cyclic voltammetry (CV) over a potential range of − 0.2 to 1.7 V vs gold reference electrode with a sweep rate of 0.2 $V.s^{-1}$ in the presence of triethylamine as a co-reactant after sandwiching the HbA1c target between antibody and APBA on the sensing area. This immunosensor demonstrated the desirable assay performance for HbA1c with a wide response range from 2 to 18% and a low detection limit (0.072%). This new strategy provides an effective method for high-performance bioanalysis and opens avenues for the development of high-sensitive and user-friendly device.

Keywords Glycated hemoglobin · Electrochemiluminescence · Metal organic framework · Nanocluster · Gold nanocluster · Paper-based electrode · Screen-printed electrode · Cyclic voltammetry

Introduction

Glycated hemoglobin (HbA1c) formed by non-enzymatic reaction of N-terminal valine residue of the Hb β-chains exposed to plasma glucose is the most important long-term index reflecting the average blood glucose level over the past 2 to 3 months [1–3]. In 2010, the American Diabetes Association (ADA) established the blood concentration of HbA1c over 5.7% and 6.5% as another criterion for the diagnosis of pre-diabetes and diabetes, respectively [1, 4, 5]. Therefore, the HbA1c determination in blood sample is important for healthcare providers to make a diagnosis and monitor long-term progress of diabetes without the influence of short-term fluctuation of blood glucose [6]. Up to now, various analytical methods have been established for

✉ Kobra Omidfar
omidfar@tums.ac.ir

1 Biosensor Research Center, Endocrinology and Metabolism Molecular–Cellular Sciences Institute, Tehran University of Medical Sciences, Tehran, Iran

2 Endocrinology and Metabolism Research Center, Endocrinology and Metabolism Research Institute, Tehran University of Medical Sciences, Tehran, Iran

3 Chemistry Department, Faculty of Science, Ayatollah Boroujerdi University, Borujerd, Iran

4 Department of Chemistry, Faculty of Physics and Chemistry, Alzahra University, Tehran, Iran

Published online: 16 August 2021

measurement of HbA1c including ion-exchange high-performance liquid chromatography (HPLC), boronate affinity chromatography, liquid chromatography-tandem mass spectroscopy (LC-MS/MS), immunoassay, and chemiluminescence flow cells [4, 7–9]. Most of these methods have common disadvantages including long time of analysis and multiple processing steps for each test, as well as they are not available in resource-limited settings owing to the lack of basic infrastructure and/or professional staff. Many types of biosensor-based diagnostic tools have been established and reported during the last decade. Among the various electrochemical, fluorescence, and colorimetric biosensors, electrochemiluminescence (ECL) assay have attracted significant research attention due to their remarkable characteristics including high sensitivity, easy controllability, low background intensity, wide dynamic range, and no necessity for excitation light source [10–12]. As an example, Zhao et al. introduced an ECL biosensor for HbA1c based on immobilization of fructosyl amino acid oxidase (FAO) onto an Au/titania nanotubes/indium-tin-oxide (ITO) and luminol [13]. In another work, Zhang et al. developed an ECL immunosensor platform for detecting HbA1c based on $[Ru(bpy)_3]^{+2}$-doped mesoporous polydopamine (MPDA) [14]. However, despite all progress in biosensing assay of HbA1c, the limitation still remains owing to the high possibility of false positive/negative and enzyme instability [13, 15].

ECL labels are important in ECL-based biosensors. During the past decade, various labels have been utilized in this system from the popular luminophore such as $[Ru(bpy)_3]^{+2}$ and luminol, to emerging nanomaterials including perovskite nanocrystals, metal nanoclusters, and carbon nitride nanosheets [16–20].

However, most existing labels still suffer from poor sensitivity, low stability, and environmental toxicity. Hence, it is still of great significance to explore new efficient and biocompatible ECL labels for the further development of the field. Bovine serum albumin–capped gold nanoclusters (BSA-AuNCs) are newly emerged luminophores with direct electron transition characteristics, uncommon optical and electrochemical properties, versatile molecule-like features, and good biocompatibility [21, 22]. However, the luminous intensity of AuNCs is much lower than those of the popular luminophores. Recently, significant research efforts have been developed to improve the luminescence intensity and stability of AuNCs, using procedures like Au nanoclusters@graphene quantum dots nanocomposite, electrocatalytic excitation and aggregation-induced emission (EEAI), and on-electrode peroxidation of AuNCs [23–25]. However, new procedures are still in urgent demand to enhance the emission and stability of AuNCs.

2D metal-organic framework (MOF) nanosheets as an emerging class of multifunctional materials have received considerable attention in recent years [12, 26]. In comparison with the conventional 3D bulk MOF crystals, 2D MOF nanosheets have superior proportions of exposed metal atoms/or catalytic active sites and higher surface area, which can ensure fast electron and mass transfer, and electrocatalytic activity [27, 28]. Such unique characteristics endow 2D MOFs with excellent potential for applications in electrochemical biosensors, catalytic, and energy storage.

Introducing nanoparticles into MOF can improve the sensitivity of assay. But, this way might not meet the requirement for enhancing the emission of AuNCs in ECL-based biosensor. One strategy that aims to address this limitation is to use a co-reaction accelerator, leading to higher concentration of reactive intermediates and promoting the reaction rate between luminophore and co-reactant, thereby producing an amplified ECL signal [29]. However, the efficiency of the accelerator reduces due to the function of separating luminophore and co-reaction accelerator. Integrating luminophore and co-reaction accelerator within a nanostructure could help to avoid this limitation and leads to high-sensitive detection of clinically biomarkers. In fact, in comparison to a single kind of material/or nanomaterial, nanocomposites can further amplify the electrode signal and improve the sensitivity of ECL system because of materials synergistic effect mutually.

Herein, an ECL assay for HbA1c detection was designed based on antibody-labeled zirconium metal-organic framework/Fe_3O_4(trimethyl chitosan)/gold nanocluster (Zr-MOF/Fe_3O_4(TMC)/AuNCs) nanocomposites as signal amplification unit and the reduced graphene oxide/aminophenylboronic acid (rGO/APBA) modified paper-based Au electrode as sensing platform. Signal amplification using Zr-MOF/Fe_3O_4(TMC)/AuNCs nanocomposites came from two strategies: First, the TMC-functionalized Fe_3O_4 nanoparticles which were integrated into the Zr-MOF nanosheets provided a high number of positively charged amine-capped nanoparticles for electrostatic interactions with negatively charged BSA-capped AuNCs to obtain the self-enhanced ECL emitter. Second, the Zr-MOF/Fe_3O_4(TMC) composites as a co-reaction accelerator promote the conversion of co-reactant TEA into the TEA free radicals ($TEA^{\bullet}$); the obtained Zr-MOF/Fe_3O_4(TMC)/AuNCs* exhibited superior ECL property. Additionally, the magnetic property of nanocomposites facilitated the bioseparation during biosensing assay. As far as we know, the synthesis or using Zr-MOF/Fe_3O_4(TMC)/AuNCs has never been reported and this multifunctional nanocomposite structures has been described for the first time in this study. As an alternative, we employed rGO/APBA paper-based gold screen-printed electrodes (Au-SPEs) for successful anchoring of HbA1c-antibody- nanocomposites in our system. Incorporation of rGO onto the paper-based Au-SPEs surface not only enhance the electrical conductivity but also lead to a better interaction between capture APBA and target HbA1c.

Materials and methods

Detailed materials and instruments can be found in the supplementary information.

Synthesis of Zr-MOF/Fe_3O_4(TMC)/AuNCs nanocomposites

A two-step procedure has been employed to synthesize the Zr-MOF/Fe_3O_4(TMC)/AuNCs nanocomposites. The synthesis process for Zr-MOF/Fe_3O_4(TMC)/AuNCs are illustrated in Scheme 1A.

Formation of Zr-MOF/Fe_3O_4(TMC) nanocomposites The synthesis of the Zr-MOF/Fe_3O_4(TMC) composites was accomplished using the procedure described by He et al., with minor modifications [30]. For this purpose, Fe_3O_4(TMC) was initially prepared by the co-precipitation method as reported in our previous works [31–33]. Detailed synthesis can be found in the supplementary information. Then, 1 mL of dispersed Fe_3O_4(TMC) nanocomplexes in DMF was added to the mixture of 10 mg $ZrCl_4$, 240 μL acetic acid, 50 μL H_2O, and 10 mg TCPP in 1 mL DMF. After 45 min of sonication, the resulting mixture was transferred into a 100-mL Teflon-lined stainless steel autoclave, sealed and kept at 120 °C for 24 h. The mixture was allowed to cool at RT, and then, the product was washed 3 times with ethanol and DI. Finally, the Zr-MOF/Fe_3O_4(TMC) nanosheets were dispersed in 0.01 M phosphate buffered saline (PBS) and stored at 4 °C.

Preparation of Zr-MOF/Fe_3O_4(TMC)/AuNCs nanocomposites The luminescent AuNCs were prepared by the green synthesis method according to previous procedures with slight modifications [23, 34]. Detailed synthesis can be found in the supplementary information. Subsequently, the appropriate amounts of Zr-MOF/Fe_3O_4(TMC) nanocomposites (1.2 mg in 1.25 mL PBS (0.01 M)) were exposed to these AuNCs (10 mL). Then, the pH was adjusted to 7.2 with 0.01 M NaOH and stirred for 24 h at RT. Ultimately, the magnetic Zr-MOF/Fe_3O_4(TMC)/AuNCs

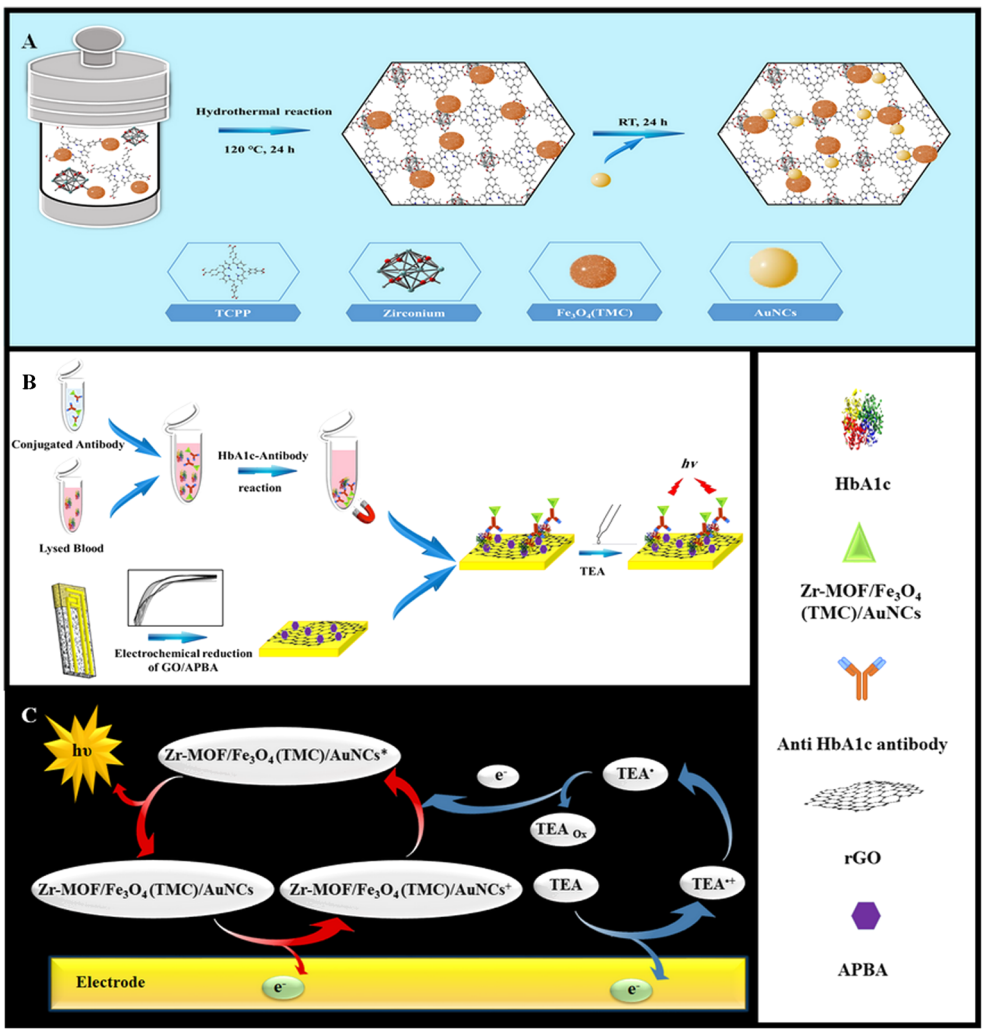

Scheme 1 Schematic representation of the Zr-MOF/Fe_3O_4(TMC)/AuNCs nanocomposite synthesis (**A**). Schematic illustration of the principal mechanism for HbA1c detection by ECL biosensing platform. Preparation of the modified paper-based Au-SPE and assay steps (**B**); ECL mechanism (**C**)

nanocomposites were collected using an external magnet and washed with DI before drying.

Conjugation of antibody on to the Zr-MOF/Fe_3O_4(TMC)/AuNCs nanocomposites

Zr-MOF/Fe_3O_4(TMC)/AuNCs and anti-HbA1c monoclonal antibody were conjugated using EDC/NHS by integrating the NH_2 groups of TMC and the COOH groups of antibodies. To do this, initially, 9.5 mg EDC and 11.5 mg NHS were dissolved in 5 mL PBS containing monoclonal antibody (5 μg). After 1 h shaking at RT, 0.5 mg of Zr-MOF/Fe_3O_4(TMC)/AuNCs was added to the mixture. The resulting solution was shaken in the dark for 5 h at RT, and then, the final product was washed several times with PBS and stored in the dark at 4 °C.

Preparation and modification of screen-printed electrode (SPE)

Cellulose acetate (CA) fibers were fabricated through electrospinning and followed by post-treatment steps according to the previously developed procedure [35]. Detailed protocols for preparation of cellulose paper and fabrication of paper-based SPE are listed in the supplementary information.

Paper-based SPE modification

Detailed protocols for immobilization of APBA on to the GO and preparation of rGO/APBA modified paper-based Au SPE are listed in the supplementary information.

Separation and quantitative determination of HbA1c

HbA1c separation from sample The separation of HbA1c from the sample was carried out by gently stirring the solution at RT. Fundamentally, various concentrations of HbA1c were prepared and then, 25 μL of antibody-Zr-MOF/Fe_3O_4(TMC)/AuNCs nanocomposites (2 $mg.mL^{-1}$) was added to each concentration (100 μL). The above products were incubated under gentle shaking for 1 h. After attachment of antibody-functionalized nanocomposites to HbA1c, the nanocomposites were separated, washed, and diluted in 100 μL PBS. Subsequently, the resulting mixture was dropped on the electrodes and the final interaction was accomplished with APBA which conjugated covalently to rGO on the surface of paper-based SPE. After 45 min of incubation, the electrodes were washed with PBS and subjected to ECL measurements.

Electrochemiluminescence measurement The performance of the biosensor was evaluated by ECL experiment. The CV was scanned from − 0.2 to 1.7 V, and a sweep rate of 0.2 $V.s^{-1}$ using a solution of 0.1 M $NaClO_4$ containing 70 mM TEA (100 μL) as the co-reactant at RT. The stability of the constructed paper-based biosensor was investigated after 14 weeks of storage at 4 °C and compared to that of newly prepared electrode. The stability of the Zr-MOF/Fe_3O_4(TMC)/AuNC nanocomposite-labeled antibody was also evaluated by storing the nanocomposite-labeled antibody in 0.1 M PB (pH 8.5) solution at 4 °C and with time-dependent fluorescence checking of the release of AuNC particles from the pores of nanocomposite-labeled antibody. Furthermore, the reproducibility, specificity, and repeatability of the biosensor were studied via measurement of HbA1c in four separate assay runs.

Real sample analysis

Whole blood samples from non-diabetic and diabetic patients were collected in tubes containing ethylenediaminetetraacetic acid (EDTA). Then, 20 μL of samples was added to 1 mL red cell lysis buffer. Afterward, HbA1c of the blood samples were measured according to the procedure described in the "Separation and quantitative determination of HbA1c" section.

Result and discussion

The goal of the present study was to offer a powerful combination of 2D MOF nanosheets, luminescent AuNCs, nanomaterials, and papers for developing a sandwich-type format paper-based ECL biosensing platform. In this work, Zr-MOF/Fe_3O_4(TMC)/AuNCs nanocomposites and paper-based SPEs were employed to design a sensitive disposable system for detecting HbA1c. The use of Zr-MOF/Fe_3O_4(TMC)/AuNCs nanocomposites, as nanocarrier and ECL detector signal to label antibody, enhances the sensitivity of the assay due to the encapsulation of large number of Fe_3O_4 (TMC) nanoparticles in the cavity of frameworks, as well as the good film-forming ability of TMC, making a welcoming positively charged surface for loading a great number of negatively charged BSA-capped AuNCs inside the Zr-MOF/Fe_3O_4(TMC) composite through electrostatic interaction [36]. Furthermore, the Zr-MOF/Fe_3O_4(TMC) composites as a co-reaction accelerator successfully stimulated the generation of active intermediate radicals, which could react with AuNCs to produce excited state species $AuNCs^*$ for generating ECL remarkably. The paper-based SPEs were subjected to some modifications including electrochemical reduction of GO to rGO and APBA immobilization which was earlier covalently attached to GO. The employ of rGO not only enhanced the surface area due to the folds but also improved the electron transfer on the electrode surface that resulted in remarkable ECL signal. Finally, antibody-labeled Zr-MOF/Fe_3O_4(TMC)/AuNCs nanocomposites were introduced to

target analyte, and on the paper-based SPEs, detection was then recorded when HbA1c interacted with APBA on the sensing area. An overview of the recognition process is presented in Scheme 1B.

Characterization of Zr-MOF/Fe_3O_4(TMC)/AuNCs nanocomposites

FTIR spectroscopy was used to investigate protein change and the analysis of the secondary structure in particular (see more details in supplementary information, Fig. S1). The quality and structural identity of fabricated nanocomposites are determined using XRD analysis (see more details in supplementary information, Fig. S2).

The size and shape of the Zr-MOF nanosheets, Zr-MOF/Fe_3O_4 (TMC) composites, and AuNCs and Zr-MOF/Fe_3O_4(TMC)/AuNCs nanocomposites were investigated by TEM (Fig. 1). As shown in Fig. 1A, Zr-MOF-TCPP exhibited a well-spread two-dimensional nanosheet structures. As can be seen in Fig. 1B, the Zr-MOF nanosheets were embedded with well-defined core/shell structures of the Fe_3O_4(TMC) nanoparticles with a mean diameter of 12 nm. The TEM image of AuNCs (Fig. 1C) shows uniform spherical shapes with a mean size in the range of 3–5 nm which were distributed in the locations marked with red circles. The layers of AuNCs on the surface of Zr-MOF/Fe_3O_4(TMC)AuNCs were not visible in TEM image, which is probably due to the small size of the AuNCs and the background of Zr-MOF/Fe_3O_4(TMC). The particle size and layer thickness for the structures were further monitored by SEM images. As shown in Fig. 1D, the Zr-MOF nanosheets were composed of many irregular two-dimensional sheets with mean sizes of 1 μm in length and a width of 300 nm. In Zr-MOF/Fe_3O_4(TMC), the Fe_3O_4(TMC) shows a scalloped structure around the MOF sheets, which indicates that there is a strong interaction between the MOF and Fe_3O_4(TMC) (Fig. 1E).

Figure 1F shows the UV-Vis spectra of Zr-MOF/Fe_3O_4(TMC) composites and AuNCs and Zr-MOF/Fe_3O_4(TMC)/AuNCs nanocomposites. As can be seen, a small absorption band was observed in samples containing Zr-MOF/Fe_3O_4(TMC) composites at 400 nm, which could be caused by the ligand to metal charge transfer [37]. A significant UV-Vis absorbance was not detected in AuNCs and Zr-MOF/Fe_3O_4(TMC)/AuNCs nanocomposites, due to the quantum size and surface functionalization with BSA [38, 39]. Figure 1F also displays the fluorescence intensity of the synthesized AuNCs and Zr-MOF/Fe_3O_4(TMC)/AuNCs nanocomposites in PBS. The maximum fluorescence emission

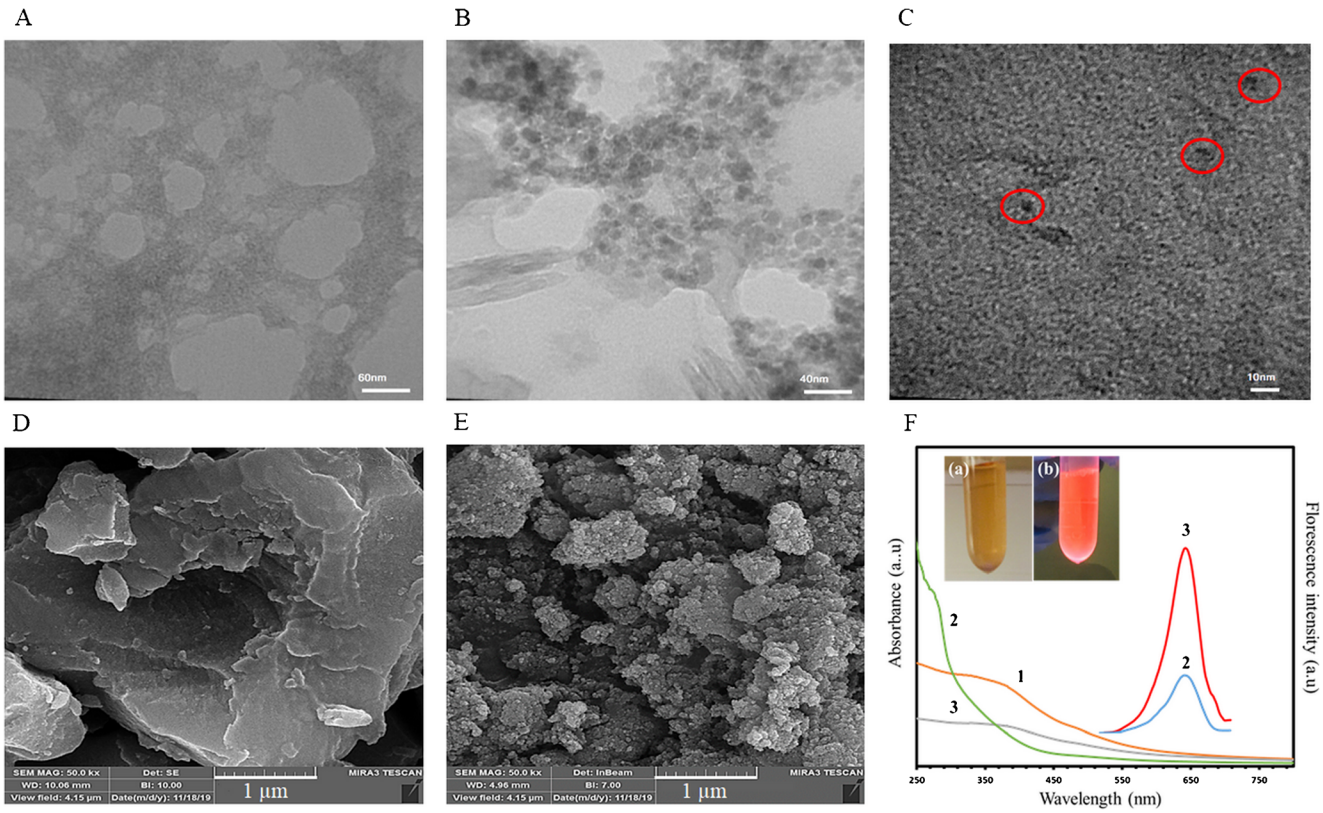

Fig. 1 TEM image of Zr-MOF nanosheets (**A**), Zr-MOF/ Fe_3O_4(TMC) composites (**B**), and AuNCs (**C**). SEM image of Zr-MOF nanosheets (**D**) and Zr-MOF/ Fe_3O_4(TMC) composites (**E**). UV-Vis and florescence intensity absorbance (**F**) of Zr-MOF/ Fe_3O_4(TMC) composites (1), AuNCs (2), and Zr-MOF/Fe_3O_4(TMC)/AuNC (3) solutions and inset image shows the Zr-MOF/ Fe_3O_4(TMC)/AuNC under visible light (a) and UV illumination (b)

spectra of AuNCs is located at about 650 nm (excitation at about 300 nm). However, the fluorescence intensity of Zr-MOF/Fe_3O_4 (TMC)/AuNCs nanocomposites was significantly higher than that of AuNCs under the same condition. According to the spherical jellium model, the emission spectra at 650 nm indicates the presence of Au_{25} clusters [34]. Moreover, the Zr-MOF/Fe_3O_4(TMC)/AuNCs nanocomposites (inset of Fig. 1F) show a dark yellow color under visible light and emit red fluorescence under the UV illumination (365 nm).

In this study, a combination of ECL and CV measurements were implemented to validate the possible luminescent mechanism of Zr-MOF/Fe_3O_4(TMC) and AuNCs and Zr-MOF/Fe_3O_4 (TMC)/AuNCs on the paper-based SPE surface (Fig. 2). The ECL signal is achieved in the presence of TEA as a co-reactant. As can be seen in Fig. 2A curve a, no distinct ECL emission could be observed from the bare Au-SPE in PBS solution, while an obvious ECL emission was obtained with TEA (curve b). The ECL signal of TEA slightly altered (curve c, f, and h) upon addition of Zr-MOF/Fe_3O_4(TMC), Fe_3O_4(TMC), and Zr-MOF to the Au-SPE, revealing that these nanocomposites had no direct effect on ECL response. In contrast, after the addition of AuNCs, an obvious ECL signal with the peak intensity of 168 a.u. could be observed (curve d), suggesting that the ECL emission certainly was formed by the excited state of AuNCs. Weak ECL signals were observed in Fe_3O_4(TMC)/AuNCs and Zr-MOF/AuNCs due to the low AuNCs loaded in nanocomposites (curves g and i). Compared with the ECL of AuNCs in the presence of TEA, the Zr-MOF/Fe_3O_4(TMC)/AuNCs nanocomposites exhibited higher ECL peak intensity at 500 a.u, declaring that the Zr-MOF/Fe_3O_4(TMC) could effectively enhance the ECL signal of AuNCs (curve e). The above phenomenon implied that AuNCs loading on Zr-MOF/Fe_3O_4(TMC) were increased in comparison with Zr-MOF/AuNCs and Fe_3O_4(TMC)/AuNCs. In the Zr-MOF/Fe_3O_4(TMC) composites, Zr-MOF provided an effective 2D nanosheet to capture a huge amount of Fe_3O_4(TMC) and subsequently AuNCs. In fact, the Zr-MOF/Fe_3O_4(TMC) as a nanocarrier and co-reaction accelerator can stimulate and also enhance the decomposition of TEA to increase the amount of $TEA^{\bullet}$, which consequently promoted the ECL reaction rate of luminophore/TEA system for boosting the ECL signal remarkably. Afterward, the electrochemical characteristic of Zr-MOF/Fe_3O_4(TMC) was evaluated to clarify the catalytic mechanism. Compared with the bare paper-based Au-SPE in PBS (Fig. 2B curve a), the CV of bare Au-SPE in 0.1 M $NaClO_4$ containing 70 mM TEA exhibited an obvious anodic peak at the potential of 1.23 V attributable to the oxidation of TEA (Fig. 2B, curve b). As Fig. 2B curve c shows, under the same conditions after the addition of Zr-MOF/Fe_3O_4(TMC) nanocomposites, the anodic peak current slightly increased due to the rise in electron transfer rate at the electrode surface. With the AuNCs, the TEA current remained high (~20% higher compared to curve b) (Fig. 2B curve d).

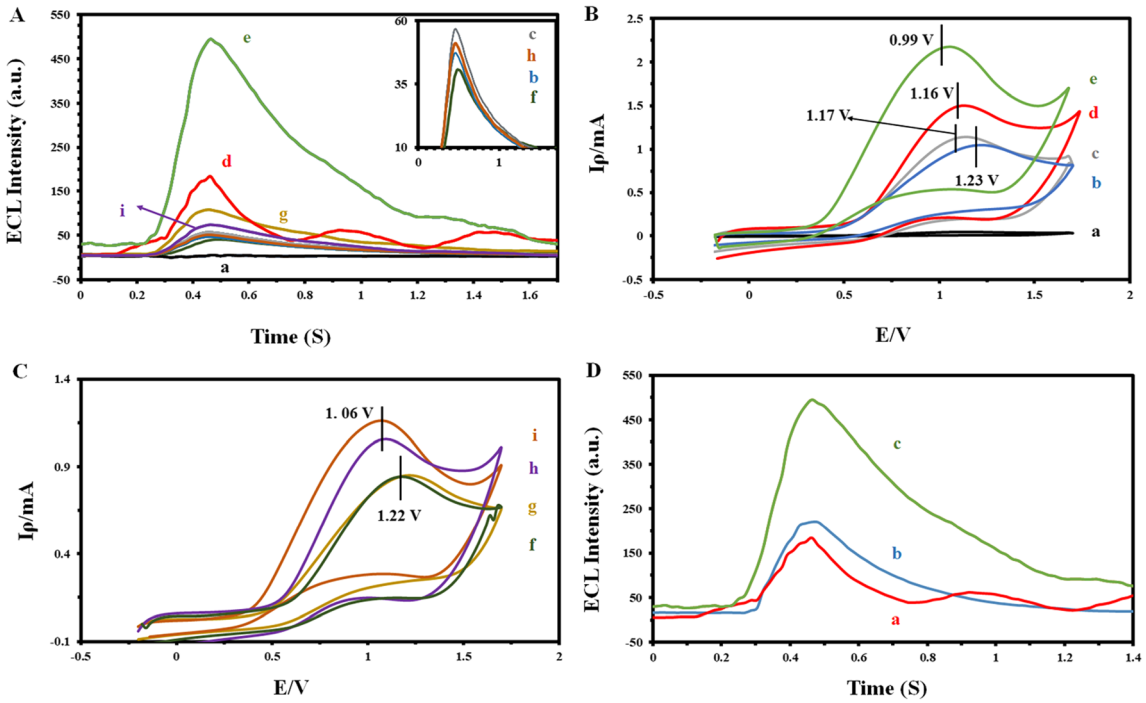

Fig. 2 ECL (**A**) and CV spectra (**B** and **C**) of the bare Au-SPE in PBS (a), bare Au-SPE in TEA (b), Zr-MOF/Fe_3O_4(TMC) nanocomposites (c), AuNCs (d), Zr-MOF/Fe_3O_4(TMC)/AuNCs nanocomposites (e), Fe_3O_4(TMC) (f), Fe_3O_4(TMC)/AuNCs (g), Zr-MOF (h), Zr-MOF/AuNCs (i) in TEA. ECL signal (D) of AuNCs (a), Zr-MOF/Fe_3O_4(TMC) with the solution of AuNCs (b) and AuNCs-loaded Zr-MOF/Fe_3O_4(TMC) (c)

The oxidation peak of Zr-MOF/Fe_3O_4(TMC)/AuNCs shifted negatively from 1.16 to 0.99 V, suggesting that the Zr-MOF/Fe_3O_4(TMC) as an accelerator can enhance the oxidation of AuNCs-TEA to form the more reductive intermediate radicals. For Fe_3O_4(TMC) and Fe_3O_4(TMC)/AuNCs, the potentials of the anodic peaks had no obvious changes from curve b, although a slight reduction in currents was observed (Fig. 2C, curves f and g). When Zr-MOF and Zr-MOF/AuNCs were measured in TEA solution, curves h and i demonstrated an obvious rise in currents, which shifted negatively from 1.23 to 1.06 compared with pure TEA solution. These results further prove that the Zr-MOF in the Zr-MOF/Fe_3O_4(TMC)/AuNCs structure could interact with TEA to accelerate the reduction of TEA for the significant enhancement of $TEA^{\bullet}$.

According to anodic ECL process of Zr-MOF/Fe_3O_4(TMC)/AuNCs in the presence of TEA, the possible ECL mechanism on the SPE could be described by Eqs. (1)–(5). During the positive potential scanning, the Zr-MOF/Fe_3O_4(TMC)/AuNCs were oxidized to Zr-MOF/Fe_3O_4 (TMC)/$AuNCs^{+}$ [Eq. (1–2)]. Meanwhile, a fraction of $TEA^{\bullet+}$ was then deprotonated to from a highly reducing radical $TEA^{\bullet}$ [Eq. (3)]. Subsequently, Zr-MOF/Fe_3O_4(TMC)/$AuNCs^{\bullet+}$ could be reduced by $TEA^{\bullet}$, producing the excited Zr-MOF/Fe_3O_4(TMC)/AuNCs* [Eq. (4)], and generating ECL emission [Eq. (5)]. In this work, the electrocatalytic reaction produced a large amount of $AuNCs^{\bullet+}$ on the surface of SPE for augmenting the ECL signal [Eq. (4)–(5)] (Scheme 1C) [40].

$$TEA\text{–}e^{-} \rightarrow TEA^{\bullet+} \quad (1)$$

$$Zr\text{–}MOF/Fe_3O_4(TMC)/AuNCs + TEA^{\bullet+} \rightarrow TEA + Zr\text{–}MOF/Fe_3O_4(TMC)/AuNCs^{+} \quad (2)$$

$$OH^{-} + TEA^{\bullet+} \rightarrow TEA^{\bullet} + H_2O \quad (3)$$

$$Zr\text{-}MOF/Fe_3O_4(TMC)/AuNCs^{+} + TEA^{\bullet} \rightarrow Zr\text{-}MOF/Fe_3O_4(TMC)/AuNCs^{*} + TEA_{Oxidate} \quad (4)$$

$$Zr\text{-}MOF/Fe_3O_4(TMC)/AuNCs^{*} \rightarrow Zr\text{-}MOF/Fe_3O_4(TMC)/AuNCs + h\upsilon \quad (5)$$

To confirm the advantages of the Zr-MOF/Fe_3O_4(TMC)/AuNCs signal probe, the ECL signal intensity of the nanobiosensor was examined using AuNcs and Zr-MOF/Fe_3O_4(TMC) with the solution of AuNCs and AuNCs-loaded Zr-MOF/Fe_3O_4(TMC) nanocomposites. These results demonstrate that the ECL intensity of the AuNCs in the presence of Zr-MOF/Fe_3O_4(TMC) was enhanced, which indicates that Zr-MOF was an accelerator for AuNCs to improve the ECL response (Fig. 2D, curves a and b). The comparison between Zr-MOF/Fe_3O_4(TMC)/AuNCs nanocomposites (Fig. 2D, curve c) and the mixture of Zr-MOF/Fe_3O_4(TMC) and AuNCs (Fig. 2D, curve b) revealed that the ECL signal intensity of the nanocomposites is more than 2-fold of the Zr-MOF/Fe_3O_4 (TMC) and AuNCs in solution. A high reaction efficiency between the formed $TEA^{\bullet+}$ and the adjacent AuNCs was achieved before the disappearance of the radical species for the Zr-MOF/Fe_3O_4(TMC)/AuNCs nanocomposites. In the solution state, the generated $TEA^{\bullet+}$ had a long diffusion distance from Zr-MOF/Fe_3O_4(TMC) and AuNCs, resulting in significantly lower reaction efficiency and ECL response.

Characterization of the modified electrode

In this study, rGO/APBA was used to modify the surface of paper-based SPE. The rGO not only enhanced the surface area to volume ratio but also improved the electron transfer on the surface of electrode, leading to signal amplification in ECL system [41, 42]. To achieve the maximum ECL sensitivity, the optimal concentrations of rGO/APBA were evaluated. For this purpose, electrochemical reduction of GO/APBA with different concentrations (20, 40, 60, 80, and 100 $\mu g.mL^{-1}$) was carried out on the surface of electrodes. As shown in Fig. S3, the maximum ECL response of biosensor was detected at 40 $\mu g.mL^{-1}$ of rGO/APBA; hence, subsequent experiments were achieved in this condition. In the next step, the function and active surface area of the rGO/APBA-modified electrodes were studied by EIS and CV in the presence of 1 mM $[Fe(CN)6]^{3-/4-}$ as a redox probe. Also, the same redox probe was used to evaluate the electron transfer resistance (R_{ct}) of the modified electrode (see more details in supplementary information, Fig. S4). ECL was also implemented to validate the effect of rGO-modified paper-based SPE surface (see more details in supplementary information, Fig. S5).

The surface morphology of modified TMC/CNs, Au-SPE, GO/APBA-Au-SPE, and rGO/APBA-Au-SPE was examined using SEM (see more details in supplementary information, Fig. S6). Surface analyses of bare Au-SPE and electrodes covered with GO/APBA and rGO/APBA were achieved using AFM (see more details in supplementary information, Fig. S7).

Optimization of detection condition

To achieve the maximum sensitivity of the ECL biosensor, the optimal concentration of antibody-conjugated Zr-MOF/Fe_3O_4(TMC)/AuNCs nanocomposites was investigated. The detailed optimization of detection condition is given in the supplementary information (Fig. S8).

Analytical performance for quantitative determination of HbA1c

To evaluate the performance of the assay, HbA1c with different concentrations were assessed using sandwich-type

model by means of the paper platform modified with rGO/APBA as sensing surface, along with Zr-MOF/Fe_3O_4(TMC)/AuNCs-labeled antibody as signal element, co-reaction accelerator, and also separating/enrichment tool. Different amounts of standard solutions were prepared by diluting the known concentrations of HbA1c 0–20% with normal plasma samples [43]. ECL analyses were performed in triplicates for each concentration by means of CV mode. The calibration curve exhibited a good relationship between the various concentrations of HbA1c from 2 to 18% and ECL responses (Fig. 3). As can be seen in Fig. 3A, the ECL intensity increased linearly with the rising of HbA1c concentrations in standard samples. The calibration curves for HbA1c biosensor are shown in Fig. 3B. The linear equation fitted to the data was $I_{ECL} = 21.885\ C\ (\%) + 384.94$ with the correlation coefficient (R^2) of 0. 0.9811. Under optimal conditions, the detection limit of this assay was calculated to be 0.072%. Table 1 displays the limit of detection and linear response range obtained by the current study and previously reported works. In comparison with some ECL-based biosensors for detecting HbA1c, the existing method offers low detection limit and good sensitivity that can be contributed to the use of Zr-MOF/Fe_3O_4(TMC)/AuNCs nanocomposites as tracing tag to label antibody and rGO/APBA on the surface of paper-based SPE as sensing element. As shown in Table 1, the LOD of this biosensor is only slightly higher than that of other types of biosensors such as impedance and amperometric; however, the linear range has been significantly wider. Furthermore, the reproducibility of the paper-based SPE was studied via measurement of HbA1c in four separate assays run. The intra-assay reproducibility of CV measurements for 3, 10, and 16% of HbA1c were calculated to be 4.1, 2.6, and 3.1%, respectively, while the inter-assay reproducibility were 3.8, 1.8, and 2.8%, respectively. These results demonstrate that we accomplished our goal of presenting an appropriate biosensor for HbA1c detection with acceptable reproducibility.

Specificity and stability of the developed paper-based SPE biosensor

The detailed investigation of specificity and stability are given in the supplementary information (Fig. S9).

Response characteristics of the developed paper-based SPE biosensor

The reliability of our paper-based SPE biosensor was evaluated by performing the assay with six whole blood samples and comparing the results with those obtained via immunoturbidimetry (IT) assay kit (Elitech clinical system SAS, France). The RSDs of the determination, calculated from three repeated measurements for diabetic and control specimens, are demonstrated in Table S1. An obtained RSD less than 4% was the indicator of appropriate accuracy of the presented biosensor and was in concordance with results of other HbA1c ECL assays in diagnostic judgment. The existence of a remarkable correlation between IT assay and our biosensor confirms that the proposed system could be utilized for the clinical diagnosis of HbA1c in real specimens.

Conclusion

A practical ECL paper-based assay for HbA1c measurement has been presented by using a double-signal amplification strategy. First, TMC functionalized Fe_3O_4 nanoparticles of Zr-MOF/Fe_3O_4 nanocomposites as nanocarrier provided a high positively charged surface for loading a large number of negatively charged BSA-capped AuNCs within the nanocomposite as nanocarrier. Second, The Zr-MOF/Fe_3O_4(TMC) as a co-reaction accelerator could increase the overall efficiency between luminophore and co-reactant for ECL signal amplification. Antibody-labeled Zr-MOF/Fe_3O_4(TMC)/AuNCs nanocomposites can selectively capture and separate the HbA1c from nonglycated Hb species and also other glycated proteins in human blood sample. Finally, the

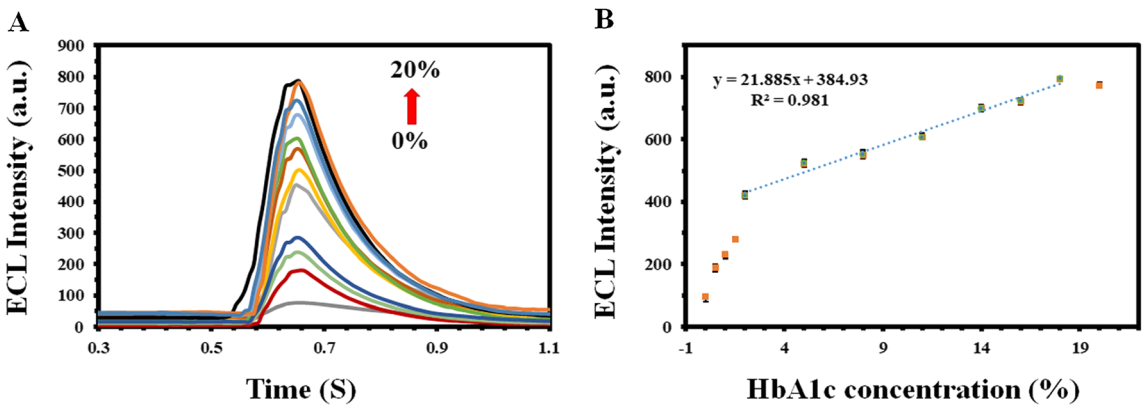

Fig. 3 ECL results for HbA1c detection using a solution of 0.1 M $NaClO_4$ containing 70 mM TEA (100 μL) at the scan rate of 0.2 $V.s^{-1}$; the concentrations of HbA1c was in the range of 0–20% (**A**). Calibration plot of HbA1c nanosensor between 0 and 20%. Each data point is the average of three replicates (**B**)

Table 1 Comparison of the analytical performance of the present ECL-based biosensor with other related HbA1c biosensors

Method	Principle	Surface modification	Label	Linearity (%)	LOD (%)	Ref.
Chemiluminescence	Boronate affinity	3-APBA	Luminol	2.5–17	–	[44]
Quartz crystal microbalance	Enzymatic	Au nanoparticles (AuNPs)		4.6–13.5	0.147	[45]
Cyclic voltammetry	Boronate affinity	4-MPBA gold nano-flowers		2–20	0.65	[46]
Impedance	Boronate affinity	3-APBA		0.1–8.36	0.024	[47]
Amperometry	Boronate affinity	3-APBA-bound conducting polymer- AuNPs		0.1–1.5	0.052	[48]
Electrochemiluminescence	immunosensor	$Ru(bpy)_3^{2+}$-doped mesoporous polydopamine		0.1–18.5	0.015	[14]
Electrochemiluminescence	Boronate affinity	rGO/APBA	Zr-MOF/Fe_3O_4 (TMC)/AuNCs	2–18	0.072	This work

suitable combination of rGO/APBA and paper-based Au-SPE provided an optimized platform for successful anchoring of HbA1c-antibody-nanocomposites in our system**.** The present combination of 2D MOF nanosheets, Fe_3O_4(TMC) nanoparticles**,** AuNCs, and rGO/APBA-modified paper-based Au electrode effectively led to fabrication of an ideal biosensing platform and provided benefits including short assay time, acceptable reproducibility, low detection limit, wide linear range, and remarkable selectivity. Consequently, it is believed that the proposed system based on the employment of Zr-MOF/Fe_3O_4(TMC) as nanocarrier and co-reaction accelerator for increasing the ECL signal can provide a new perspective for signal amplification in ECL biosensor.

At present, our system was limited at the medical laboratory setting. To develop a sensitive and biocompatible device for the detection of HbA1c level at anywhere and anytime, we need to realize the integration of the detection system and combine our system with a portable measuring system.

Supplementary Information The online version contains supplementary material available at https://doi.org/10.1007/s00604-021-04959-y.

Acknowledgments The authors thank MAN company heads for their assistance on sample collection and providing HbA1c assay kit in this work.

Funding Research reported in this publication was supported by a grant from the Endocrinology and Metabolism Research Center of Tehran University of Medical Sciences in Iran.

Declarations

All procedures performed in this study were in accordance with the ethical standards of the Tehran University of Medical Sciences and with the 1964 Helsinki declaration.

Conflict of interest The authors declare no competing interests.

References

1. Ahmadi A, Kabiri S, Omidfar K (2020) Advances in HbA1c biosensor development based on field effect transistors: a review. IEEE Sensors J 20:8912–8921
2. Wang B, Anzai J-I (2015) Recent progress in electrochemical HbA1c sensors: a review. Materials 8:1187–1203
3. Nathan DM, Singer DE, Hurxthal K, Goodson JD (1984) The clinical information value of the glycosylated hemoglobin assay. N Engl J Med 310:341–346
4. Eissa S, Zourob M (2017) Aptamer-based label-free electrochemical biosensor array for the detection of total and glycated hemoglobin in human whole blood. Sci Rep 7:1–8
5. Lipska KJ, Krumholz HM (2017) Is hemoglobin A1c the right outcome for studies of diabetes? Jama 317:1017–1018
6. Bergenstal RM, Beck RW, Close KL, Grunberger G, Sacks DB, Kowalski A, Brown AS, Heinemann L, Aleppo G, Ryan DB, Riddlesworth TD, Cefalu WT (2018) Glucose management indicator (GMI): a new term for estimating A1C from continuous glucose monitoring. Diabetes Care 41:2275–2280
7. Tanaka J, Ishige Y, Iwata R, Maekawa B, Nakamura H, Sawazaki T, Kamahori M (2018) Direct detection for concentration ratio of HbA1c to total hemoglobin by using potentiometric immunosensor with simple process of denaturing HbA1c. Sensors Actuators B Chem 260:396–399
8. Chandalia H, Krishnaswamy P (2002) Glycated hemoglobin. Curr Sci 83:1522–1532
9. Liu A, Xu S, Deng H, Wang X (2016) A new electrochemical hba1c biosensor based on flow injection and screen-printed electrode. Int J Electrochem Sci 11:3086–3094
10. Yang JK, Lee HR, Hwang IJ, Kim HI, Yim D, Kim JH (2018) Fluorescent 2D WS2 Nanosheets bearing chemical affinity elements for the recognition of glycated hemoglobin. Adv Healthcare Mater 7:1701496
11. Guo W, Ding H, Gu C, Liu Y, Jiang X, Su B, Shao Y (2018) Potential-resolved multicolor electrochemiluminescence for multiplex immunoassay in a single sample. J Am Chem Soc 140:15904–15915
12. Khoshfetrat SM, Khoshsafar H, Afkhami A, Mehrgardi MA, Bagheri H (2019) Enhanced visual wireless electrochemiluminescence immunosensing of prostate-specific antigen based on the luminol loaded into MIL-53 (Fe)-NH2 accelerator and hydrogen evolution reaction mediation. Anal Chem 91:6383–6390
13. Zhao Q, Tang S, Fang C, Tu Y-F (2016) Titania nanotubes decorated with gold nanoparticles for electrochemiluminescent biosensing of glycosylated hemoglobin. Anal Chim Acta 936:83–90

14. Zhang P, Zhang Y, Xiong X, Lu Y, Jia N (2020) A sensitive electrochemiluminescence immunoassay for glycosylated hemoglobin based on Ru (bpy) 32+ encapsulated mesoporous polydopamine nanoparticles. Sensors Actuators B Chem 321: 128626
15. Lin H, Yi J (2017) Current status of HbA1c biosensors. Sensors 17: 1798
16. Wang D, Zhou J, Guo L, Qiu B, Lin Z (2020) A surface-enhanced electrochemiluminescence sensor based on au-SiO 2 core–shell nanocomposites doped with Ru (bpy) 3 2+ for the ultrasensitive detection of prostate-specific antigen in human serum. Analyst 145:132–138
17. Khoshfetrat SM, Bagheri H, Mehrgardi MA (2018) Visual electrochemiluminescence biosensing of aflatoxin M1 based on luminol-functionalized, silver nanoparticle-decorated graphene oxide. Biosens Bioelectron 100:382–388
18. Jia F-F, Zhong H, Zhang WG, Li XR, Wang GY, Song J, Cheng ZP, Yin JZ, Guo LP (2015) A novel nonenzymatic ECL glucose sensor based on perovskite LaTiO3-Ag0. 1 nanomaterials. Sensors Actuators B Chem 212:174–182
19. Zhang C, Fan Y, Zhang H, Chen S, Yuan R (2019) An ultrasensitive signal-on electrochemiluminescence biosensor based on Au nanoclusters for detecting acetylthiocholine. Anal Bioanal Chem 411:905–913
20. Jian X, Li Y, Zhao C, Chang Y, Gao Z, Song Y-Y (2020) Introducing graphitic carbon nitride nanosheets as supersandwich-type assembly on porous electrode for ultrasensitive electrochemiluminescence immunosensing. Anal Chim Acta 1097:62–70
21. Zhu M, Lanni E, Garg N, Bier ME, Jin R (2008) Kinetically controlled, high-yield synthesis of Au25 clusters. J Am Chem Soc 130: 1138–1139
22. Jiang W, Yin H, Zhou Y, Duan J, Li H, Wang M, Waterhouse GI, Ai S (2018) A novel electrochemiluminescence biosensor for the detection of 5-methylcytosine, TET 1 protein and β-glucosyltransferase activities based on gold nanoclusters-H2O2 system. Sensors Actuators B Chem 274:144–151
23. Zhang X-L, Li X, Li X-T, Gao Y, Feng F, Yang G-J (2019) Electrochemiluminescence sensor for pentoxifylline detection using au nanoclusters@ graphene quantum dots as an amplified electrochemiluminescence luminophore. Sensors Actuators B Chem 282:927–935
24. Peng H, Huang Z, Deng H, Wu W, Huang K, Li Z, Chen W, Liu J (2019) Dual enhancement of gold nanocluster Electrochemiluminescence: electrocatalytic excitation and aggregation-induced emission. Angew Chem 59:9982–9985
25. Li D, Wang G, Mei X (2020) Diagnosis of cancer at early stages based on the multiplex detection of tumor markers using metal nanoclusters. Analyst 145:7150–7161
26. Zhou Y, Chen M, Zhuo Y, Chai Y, Xu W, Yuan R (2017) In situ electrodeposited synthesis of electrochemiluminescent Ag nanoclusters as signal probe for ultrasensitive detection of cyclin-D1 from cancer cells. Anal Chem 89:6787–6793
27. Gan X, Han D, Wang J, Liu P, Li X, Zheng Q, Yan Y (2020) A highly sensitive electrochemiluminescence immunosensor for h-FABP determination based on self-enhanced luminophore coupled with ultrathin 2D nickel metal-organic framework nanosheets. Biosens Bioelectron 171:112735
28. Liu X, Yan Z, Zhang Y, Liu Z, Sun Y, Ren J, Qu X (2019) Two-dimensional metal–organic framework/enzyme hybrid Nanocatalyst as a benign and self-activated cascade reagent for in vivo wound healing. ACS Nano 13:5222–5230
29. Zhou J, Li Y, Wang W, Tan X, Lv Z, Han H (2020) Metal-organic frameworks-based sensitive electrochemiluminescence biosensing. Biosens Bioelectron 164:112332
30. He T, Ni B, Zhang S, Gong Y, Wang H, Gu L, Zhuang J, Hu W, Wang X (2018) Ultrathin 2D zirconium metal–organic framework nanosheets: preparation and application in photocatalysis. Small 14: 1703929
31. Daneshpour M, Omidfar K, Ghanbarian H (2016) A novel electrochemical nanobiosensor for the ultrasensitive and specific detection of femtomolar-level gastric cancer biomarker miRNA-106a. Beilstein J Nanotechnol 7:2023–2036
32. Shirazi H, Daneshpour M, Kashanian S, Omidfar K (2015) Synthesis, characterization and in vitro biocompatibility study of Au/TMC/Fe3O4 nanocomposites as a promising, nontoxic system for biomedical applications. Beilstein J Nanotechnol 6:1677–1689
33. Omidfar K, Darzianiazizi M, Ahmadi A, Daneshpour M, Shirazi H (2015) A high sensitive electrochemical nanoimmunosensor based on Fe3O4/TMC/Au nanocomposite and PT-modified electrode for the detection of cancer biomarker epidermal growth factor receptor. Sensors Actuators B Chem 220:1311–1319
34. Xie J, Zheng Y, Ying JY (2009) Protein-directed synthesis of highly fluorescent gold nanoclusters. J Am Chem Soc 131:888–889
35. Ahmadi A, Khoshfetrat SM, Kabiri S, Fotouhid L, Dorrajid PS, Omidfar K (2021) Impedimetric paper-based enzymatic biosensor using electrospun cellulose acetate nanofiber and reduced graphene oxide for detection of glucose from whole blood. IEEE Sensors J 21:9210–9217
36. Barman MK, Paramanik B, Bain D, Patra A (2016) Light harvesting and white-light generation in a composite of carbon dots and dye-encapsulated BSA-protein-capped gold nanoclusters. Chem-Eur J 22:11699–11705
37. Govindaraju S, Puthiaraj P, Lee M-H, Yun K (2018) Photoluminescent AuNCs@ UiO-66 for ultrasensitive detection of mercury in water samples. ACS Omega 3:12052–12059
38. Kawasaki H, Yamamoto H, Fujimori H, Arakawa R, Iwasaki Y, Inada M (2010) Stability of the DMF-protected Au nanoclusters: photochemical, dispersion, and thermal properties. Langmuir 26: 5926–5933
39. Govindaraju S, Ankireddy SR, Viswanath B, Kim J, Yun K (2017) Fluorescent gold nanoclusters for selective detection of dopamine in cerebrospinal fluid. Sci Rep 7:40298
40. Zhai Q, Xing H, Zhang X, Li J, Wang E (2017) Enhanced Electrochemiluminescence behavior of gold–silver bimetallic nanoclusters and its sensing application for mercury (II). Anal Chem 89:7788–7794
41. Syedmoradi L, Ahmadi A, Norton ML, Omidfar K (2019) A review on nanomaterial-based field effect transistor technology for biomarker detection. Microchim Acta 186:739
42. Khodaei R, Ahmady A, Khoshfetrat SM, Kashanian S, Tavangar SM, Omidfar K (2019) Voltammetric immunosensor for E-cadherin promoter DNA methylation using a Fe 3 O 4-citric acid nanocomposite and a screen-printed carbon electrode modified with poly (vinyl alcohol) and reduced graphene oxide. Microchim Acta 186:170
43. Kwak J, Park HJ, Lee SS (2018) Gold nanoparticle-based novel biosensors for detecting glycated hemoglobin. Bull Kor Chem Soc 39:156–160
44. Ahn K-S, Lee JH, Park J-M, Choi HN, Lee W-Y (2016) Luminol chemiluminescence biosensor for glycated hemoglobin (HbA1c) in human blood samples. Biosens Bioelectron 75:82–87

45. Park HJ, Lee SS (2018) A quartz crystal microbalance-based biosensor for enzymatic detection of hemoglobin A1c in whole blood. Sensors Actuators B Chem 258:836–840
46. Wang X, Su J, Zeng D, Liu G, Liu L, Xu Y, Wang C, Liu X, Wang L, Mi X (2019) Gold nano-flowers (Au NFs) modified screen-printed carbon electrode electrochemical biosensor for label-free and quantitative detection of glycated hemoglobin. Talanta 201: 119–125
47. Boonyasit Y, Laiwattanapaisal W, Chailapakul O, Emnéus J, Heiskanen AR (2016) Boronate-modified interdigitated electrode array for selective impedance-based sensing of glycated hemoglobin. Anal Chem 88:9582–9589
48. Kim D-M, Shim Y-B (2013) Disposable amperometric glycated hemoglobin sensor for the finger prick blood test. Anal Chem 85: 6536–6543